Phase formation and lattice strain in superconducting compound $Y_{1-x}La_xBa_2Cu_3O_y$ $(0 \leqslant x \leqslant 1)$

A. Gantis and M. Calamiotou
Solid State Physics Department, School of Physics, University of Athens, GR-15784 Athens, Greece

D. Palles, D. Lampakis, and E. Liarokapis
Department of Physics, National Technical University of Athens, 157 80 Athens, Greece

(Received 9 January 2003; revised manuscript received 13 May 2003; published 6 August 2003)

We study the formation and evolution of phases in the La substituted $Y_{1-x}La_xBa_2Cu_3O_y$ [(Y–La)123] superconductors from XRD and Raman measurements. We find characteristic modifications in the interatomic distances, bond valence sum (BVS) values and crystallite microstrains, which correlate with corresponding features of the micro-Raman spectra at nominal La compositions $x=0.2$, 0.5, and 0.8. Based on the Raman spectra we conclude that two phases appear, an intermediate of chemical formula $Y_{1-x}La_xBa_2Cu_3O_y$ with x values less than nominal, and another phase of pure La123 with partial substitution of La for Ba and reduced T_c. The crystallographic changes and the reduction of T_c can be interpreted based on the formation of this pure La123 subphase upon La doping.

DOI: 10.1103/PhysRevB.68.064502 PACS number(s): 74.25.Kc, 74.72.−h, 61.10.Nz, 64.75.+g

I. INTRODUCTION

Rare-earth substituted YBCO systems have been extensively studied in order to understand the origin of the strong modification of their superconducting properties in the case of Pr substitution. The $YBa_2Cu_3O_y$ (Y123) high T_c superconductor has an oxygen deficient strained tri-perovskite structure, the internal strains playing an important role in the physical properties of the system. The replacement of Y by another rare earth R results in a linear shrinkage of the crystallographic axes with increasing atomic number of R, due to the size-effect and the lanthanide contraction behavior.[1,2] However, subtle crystal structure changes and internal strains are due to more complicated effects, besides the size-effect, such as valence-induced carrier redistribution when the dopant rare earth occupies other than the Y site or/and oxygen disordering and stoichiometry. These effects are more pronounced for the light rare earths, especially Pr and La. Unit cell values for the Pr123 compound, which is not a bulk superconductor, and for La123, which has a T_c between 45 K and 93 K (Refs. 3 and 4) deviate from the lanthanide linear trend.[1,2] Structural data reported in various papers for the La123 compound are scattered, in contrast to the Y123 superconductor, which has a well-established structure with interatomic bond distances and bond valence sum values studied thoroughly.[5–7] The nominal La123 compound has been shown to be an end member of the solid solution family $La_{1+x}Ba_{2-x}Cu_3O_y$, with physical properties being sensitive to the preparation conditions. The scattered values of T_c observed for the nominal La123 compound are mainly attributed to the disorder of La, Ba, and the chain oxygen atoms, as well as the uncontrolled oxygen stoichiometry.[3,4] Such a disorder is expected to introduce additional internal strains (changes of the different interatomic distances) in the lattice of La123.

In a previous paper we have shown that in the $(La_{0.5}R_{0.5})123$ mixed compounds characteristic changes in the interatomic distances are indicative of La induced internal strains in the unit cell. Moreover, relaxation of the internal strains can result in phase separation of the mixed system with average ionic radius 1.09 Å, which corresponds to the compound $(La_{0.5}Y_{0.5})123$.[8] Therefore, the study of the solid solution $Y_{1-x}La_xBa_2Cu_3O_y$ [(Y–La)123] $(0 \leqslant x \leqslant 1)$ seems to be essential in order to examine the relation between La induced internal strains, phase separation, size of the ion and superconductivity.

The superconductive behavior of $La_xY_{1-x}Ba_2Cu_3O_y$ $(0.05 \leqslant x \leqslant 0.75)$ solid solution has been reported so far only in one paper by Ganapathi *et al.*[9] They have found that for $x<0.5$ the system behaves more like a pure Y123 superconductor oxide while for $x>0.5$ the system starts behaving like a La123 system with high sensitivity of superconducting properties on the preparation conditions. However, a detailed investigation of lattice distortions and phase separation effects induced by La doping in the Y123 superconductor, which could give some better insight in the physical properties of the solid solution and the end member La123, has not been reported so far.

In this work we study with XRD Rietveld analysis the interatomic distances and bond valence sum variation with La doping x $(0.01 \leqslant x \leqslant 1)$ in the $Y_{1-x}La_xBa_2Cu_3O_y$. X-ray line broadening analysis has been also used to obtain crystallite microstrains associated with La–Y inhomogeneities (phase separation) in this solid solution. Raman spectroscopy has been used to investigate the separation into phases and the possible substitution of La for Ba. Characteristic changes in the B_{1g} Raman active phonon showed the formation of a pure La123 subphase, the amount of which correlates very well with structural modifications. The observed reduction in T_c is associated with the development of the pure La123 phase and not with the total amount of La, implying the important role of phase separation effects when interpreting the superconducting properties of rare-earth substituted YBCO.

II. EXPERIMENT

Polycrystalline ceramic samples $Y_{1-x}La_xBa_2Cu_3O_y$ have been prepared from high purity (99.999%) powders La_2O_3,

TABLE I. Rietveld refinements of XRD data for $Y_{1-x}La_xBa_2Cu_3O_y$. The space group is *Pmmm* with Ba($\frac{1}{2},\frac{1}{2},z$), La($\frac{1}{2},\frac{1}{2},\frac{1}{2}$), Y($\frac{1}{2},\frac{1}{2},\frac{1}{2}$), Cu(1)(0,0,0), Cu(2)(0,0,z), O(1)(0,0,z), O(2)(0,$\frac{1}{2}$, z), O(3)($\frac{1}{2}$,0,z), and O(4)(0,$\frac{1}{2}$,0). Also shown T_c, ΔT_c, oxygen content (y), and shielding fraction (SF).

	$x=0.01$	$x=0.10$	$x=0.20$	$x=0.30$	$x=0.40$	$x=0.50$	$x=0.60$	$x=0.70$	$x=0.80$	$x=0.90$	$x=1.00$
z(Ba)	0.1834(3)	0.1825(3)	0.1827(3)	0.1834(3)	0.1816(5)	0.1816(4)	0.1807(5)	0.1793(5)	0.1809(6)	0.1802(5)	0.1796(7)
z(Cu2)	0.3561(6)	0.3566(7)	0.3537(6)	0.3533(6)	0.351(1)	0.3516(9)	0.351(1)	0.348(1)	0.348(1)	0.347(1)	0.346(2)
z(O1)	0.162(3)	0.161(3)	0.159(2)	0.160(3)	0.160(5)	0.162(5)	0.159(5)	0.156(5)	0.163(7)	0.161(5)	0.164(7)
z(O2)	0.377(2)	0.385(2)	0.376(2)	0.362(3)	0.359(4)	0.367(4)	0.367(4)	0.383(4)	0.360(5)	0.364(4)	0.360(6)
z(O3)	0.383(2)	0.369(2)	0.381(2)	0.382(2)	0.382(3)	0.380(3)	0.388(3)	0.377(3)	0.394(4)	0.386(3)	0.416(4)
a(Å)	3.8218(4)	3.8239(4)	3.8301(2)	3.8385(4)	3.8502(6)	3.8430(6)	3.8561(3)	3.8666(3)	3.8694(3)	3.8822(3)	3.8911(3)
b(Å)	3.8875(4)	3.8866(5)	3.8874(3)	3.8927(5)	3.9034(7)	3.8992(7)	3.9095(5)	3.9165(5)	3.9167(5)	3.9269(4)	3.9330(8)
c(Å)	11.677(1)	11.676(1)	11.685(1)	11.702(2)	11.732(2)	11.717(2)	11.749(2)	11.778(1)	11.777(2)	11.805(1)	11.808(3)
R(%)	6.28	6.15	5.43	6.15	7.39	7.32	7.19	6.13	7.23	7.02	8.83
R_{wp} (%)	8.25	6.80	6.70	7.15	8.69	8.42	8.46	7.78	9.14	8.94	11.09
R_{exp} (%)	5.51	4.75	4.62	4.54	5.77	5.70	5.38	5.47	5.60	5.80	6.12
R_{Bragg} (%)	5.73	6.24	4.60	6.50	7.79	8.82	6.89	6.02	6.19	6.84	8.64
$BaCuO_2$ (%)	0.97	2.33	4.16	4.51	5.30	5.80	7.57	6.11	5.62	6.42	5.65
y	7.07(2)	6.97(2)	6.90(2)	6.92(2)	6.92(2)	7.01(2)	6.99(2)	6.98(2)	7.00(2)	7.05(2)	6.95(2)
T_c	91	91	84	83	85	86	85	82	81	79	74
ΔT_c	30	36	44	43	52	45	50	50	51	52	52
x	0.004	0.092	0.182	0.282	0.385	0.472	0.617	0.727	0.827	0.938	0.883
SF(%)	81	83	71	54	49	56	48	49	60	40	44

Y_2O_3, $BaCO_3$, and CuO by the solid-state reaction technique. In order to prevent contamination from CO_2 and moisture, the initial La_2O_3 powder was heat treated and then all starting materials have been mixed according to the nominal composition, ground, pressed into pellets, and calcinated at 920 °C for 20 h in an oxygen atmosphere. The pellets have been reground, repressed, and further thermally treated in oxygen flow for 20 h (four times) at 940, 960, 980, and 990 °C, respectively. According to the XRD examination the pellets consisted of a single crystalline phase and the commonly found $BaCuO_2$ phase. It is known that the chemistry of the La–Ba–Cu–O system is different from that of Y123 having a large number of ternary compound and solid solution series. Sintering in inert atmosphere is necessary for the synthesis of single phase La123.[3,4] Therefore, sintering of the samples has been performed in He atmosphere at 950 °C for about 30 h. The samples have been then cooled down to 500 °C in the furnace and annealed at that temperature for 15 h under flowing oxygen. The process (sintering and annealing) has been repeated until the amount of $BaCuO_2$ was reduced to a percentage lower than 8%.

11 samples have been prepared with the composition corresponding to $x=0.01$, 0.10, 0.20, 0.30, 0.40, 0.50, 0.60, 0.70, 0.80, 0.90, 1.00. The superconducting critical temperature has been determined using a SQUID magnetometer in the Zero Field Cooled (ZFC) mode. Oxygen stoichiometry has been obtained by a volumetric method, taking into account the presence of the $BaCuO_2$ impurity phase for each sample.[10]

X-ray diffraction measurements at room temperature have been carried out on a Siemens D5000 powder diffractometer with Cu $K\alpha$ radiation and a graphite secondary monochromator. The XRD patterns have been collected in a standard two-cycle goniometer in Bragg-Brentano para-focusing geometry by step scanning mode. A step size of 0.03° and a counting time of about 15 s/step have been used.

Micro-Raman spectra have been measured at room temperature with a Jobin-Yvon T64000 triple spectrometer equipped with a liquid nitrogen cooled CCD and a microscope (magnification $\times 100$). The 488 nm and 514.5 nm lines of an Ar^+ laser and the 530.9 nm of a Kr^+ were used at low power (<0.2 mW) focused on a 1–2 μm spot size. Accumulation times were 1.5 and 3 h for the zz and $xx(yy)$ scattering geometries, respectively.

A. Results

The XRD patterns of all samples have been analyzed with the Rietveld method using the program RIET,[11] assuming for each sample two phases, the main (Y–La)123 and the impurity phase $BaCuO_2$. The refinement has been carried out (120 Bragg reflections, 1670 points) using for the (Y–La)123 phase the starting crystal structure model of Y123 (space group *Pmmm*).[5] Each reflection peak has been assumed to be described by a Pearson VII profile shape function with split FWHM and shape. Sample preferred orientation has been set to the vector 00l using the March function.[12] For the $BaCuO_2$ impurity phase, the structural parameters reported in Ref. 13 have been used without refinement, while the corresponding scale factor was refined and the content of the impurity phase was estimated according Hill and Howard[14] for each sample (Table I).

Due to the difference in the scattering factors of Y and La the site occupancy at the Y site by La could be refined in the (Y–La)123 phase. Results shown in Fig. 1(a) indicate that the average amount of La in the Y site coincide with the

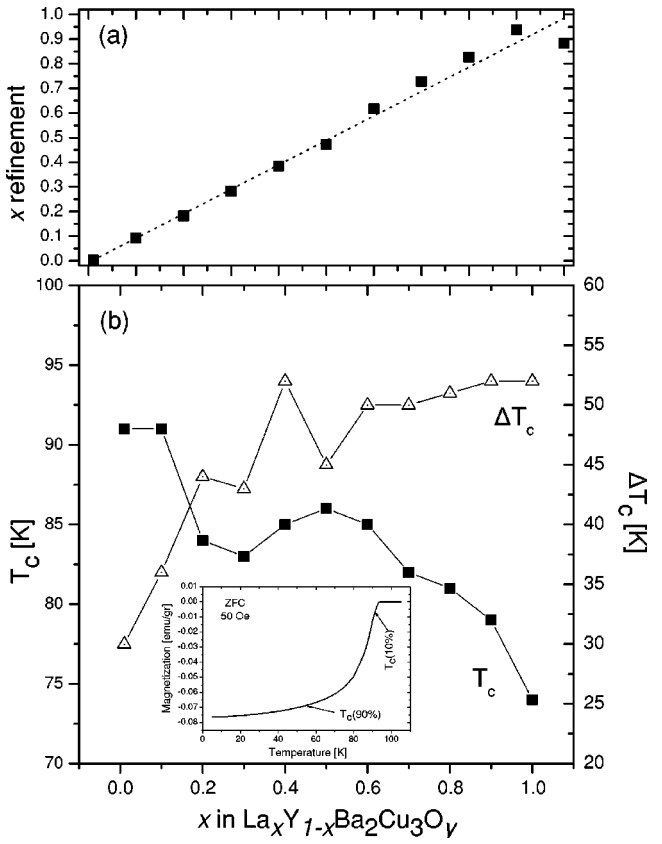

FIG. 1. (a)The site occupancy at the Y site by La from Rietveld refinement vs the nominal stoichiometry, (b) The transition temperature and the transition width ΔT_c as a function of La doping x. The inset shows a typical ZFC magnetization vs temperature curve for $x=0.1$ (H=50 Oe).

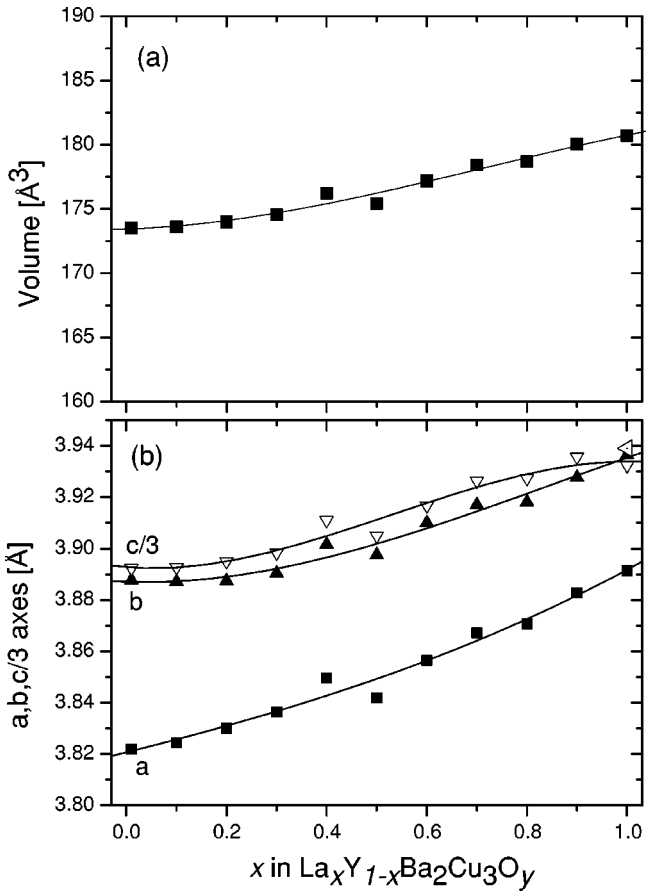

FIG. 2. Dependence of the cell volume (a) and a, b, $c/3$ unit cell values (b) of the (Y–La)123 compounds on the La content x. Solid lines are fits of the data with a third order polynomial.

nominal composition for all samples except for La123 ($x=1.0$), which is La deficient. This means that the La123 phase has vacancy and/or antisite La_{Ba} defects. From neutron diffraction data[2] it is known that La can occupy also the Ba site, however this cannot be detected in our samples by refining the corresponding site occupancies due to the similar x-ray scattering factors for the two elements. An attempt to refine a mixed Ba/La occupation factor resulted in unrealistic values. In a preliminary refinement we have also tried to include in the refinement a third phase, the tetragonal $La_{1+x}Ba_{2-x}Cu_3O_{7-\delta}$, following the results obtained by Izumi *et al.*[4] for the nominal La123. For samples with $x<0.7$ the refined corresponding scale factors indicated that no such tetragonal phase was present. For $x\geqslant 0.7$ we have obtained improved *R*-factors when including in the refinement the tetragonal phase. However the obtained values for some interatomic distances and especially the fractional coordinate z for Ba of the main La–Y123 phase were unrealistic. This indicates that the improvement of the refinement assuming the presence of a ''tetragonal'' $(LaBa)_3Cu_3O_{7-\delta}$ phase could represent the contribution of an inhomogeneity in those samples as pointed out also by Izumi *et al.*[4] Therefore any La/Ba disorder can be eventually indirectly manifested as a change of different bond lengths and bond valence sum values at the Ba site of the orthorhombic phase as discussed below.

Table I presents the structural parameters of the $Y_{1-x}La_xBa_2Cu_3O_y$ compounds as determined from the final Rietveld refinement. In Table I are also shown the oxygen content y, the T_c values, the corresponding diamagnetic transition widths ΔT_c (10%–90%) and the (%) shielding fraction SF, estimated from the ZFC magnetic susceptibility data [inset Fig. 1(b)]. All samples are optimally doped or overdoped ($y=6.9-7.07$) with a slight tendency of increased amount of oxygen with increasing La concentration. So, samples with $x\geqslant 0.5$ have on average higher oxygen content ($y=6.98-7.05$) compared to the samples with $0.01<x<0.5$. The transition temperature (T_c) is decreasing from 92 K (for $x=0.01$) to 74 K (for $x=1$). The decrease is not linear with La doping x showing two plateaus [Fig. 1(b)], the first at 92 K for $x<0.2$ and the second at approximately 85 K for $0.2\leqslant x\leqslant 0.7$. The ΔT_c increases considerably to an asymptotic value of 50 K for $x=0.4$ [Fig. 1(b)]. This should reflect also the coexistence of phases as discussed below.

The unit cell volume and parameters increase with La doping in agreement with the larger La^{3+} ($r=1.16$ Å) replacing the smaller Y^{3+} ($r=1.019$ Å) (Fig. 2). The values of the end members with $x=0$ ($YBa_2Cu_3O_{6.93}$) (Ref. 5) and $x=1$ ($LaBa_2Cu_3O_{6.95}$) (Ref. 3) agree with our values. However for the small substitutional limit ($x\lesssim 0.2$) a deviation of the unit cell volume from the linear behavior (Vegard's law)

is observed. The same deviation from the linear behavior has been observed for the $c/3$ and to a lesser extent for the b lattice constant. It is interesting that the c-axis shows a slight deviation from linearity towards the end member La123 too [Fig. 2(b)], probably reflecting the partial substitution of La for the larger Ba ion in the $2t(1/2,1/2,z)$ site[15] as discussed below.

La replacing Y in the Y123 structure results in a tensile strain of the unit cell, which is 1.8% for the a, 1.2% for the b, and 1.1% for the c axis. Orthorhombic strain, defined as $(b-a)/(b+a)$, is generally decreasing with La doping [Fig. 3(a)] with a jump to higher values at $x=0.5$. The latter may be related to the observed higher oxygen content of the samples with $x \geqslant 0.5$.

In order to have an insight in the internal strains induced by the La doping we have calculated different interatomic distances with oxygen atoms labeled as follows: O(1) apical, O(2) plane along the b axis, O(3) plane along the a axis, and O(4) and O(5) basal plane along the b and a axis respectively. An increase (decrease) is observed for Cu(2)–Cu(2)(Cu(2)–Cu(1)) bond distance with La doping [Fig. 3(b)]. Most of the stress introduced by the larger La replacing the smaller Y atom in the $1h$ (1/2,1/2,1/2) site of the unit cell, seems to be accommodated by the Cu(2)–Cu(2) bond, which is increasing by 8.3% while the Cu(2)–Cu(1) bond is decreasing only by 1.6%.

Internal strains concerning the bonds with the apical oxygen are expected to be important in the La doped system since the site of the apical oxygen is sensitive to size effects, to the presence of excess oxygen on the basal plane, and the La/Ba disorder. The larger Cu(2)–O(1) bond distance is decreasing with La doping while the smaller Cu(1)–O(1) bond distance is almost constant with a tendency to slight increase for the higher ($x \geqslant 0.8$) La substitution values [Fig. 3(c)]. The substitution of Y by the larger La atom induces an internal chemical pressure in the unit cell. Internal strains in Y123 lattice induced by a 2% compressive uniaxial strain along the a, b, and c axis have been theoretically calculated. Pickett[16] has found that a 2% c-axis compression decreases the short Cu(1)–O(1) bond by only 0.018 Å and the long Cu(2)–O(1) bond by nearly seven times as much (0.124 Å) being in agreement with our results. The scattered values for $x>0.6$ indicate that the internal strains of the apical O(1) for those samples at the high La substitution limit are additionally affected by other factors than the size effect. These interatomic distances are also sensitive to the occupancy of the sites O(4) and O(5) which may be induced by the La/Ba replacement, and the scattered values are partially due to the variations of the oxygen doping.

According to the calculations of Pickett,[16] the strain driven displacements of atoms (internal strains), which are substantial in the Y123 structure, are those of the Cu(2) and O(3) atoms while those of O(2) and Ba are comparatively small. The Cu(2)–O(3) is increasing with x while little effect is observed for the Cu(2)–O(2) distance [Fig. 3(d)]. The latter could be understood taking into account that the O(2) atom is situated along the more interlinked [due to the O(4) chains] b-axis and is in agreement with the above calculations. However the increase of the Cu(2)–O(3) distance is not linear with La doping x. The La123 phase ($x=1$) exhibits a high Cu(2)–O(3) bond value indicating that the La ion induces large tensile internal strains in the Cu(2)–O(3) bonds in agreement with the previous results.[8] Therefore, at $0.2<x \leqslant 0.8$ the two bonds become similar due to the La123 phase formation as will be discussed bellow.

Following an initial small increase (decrease), at $x=0.2$ the Y/La–O(3) (Ba–O(3)) distance is decreasing (increasing) with La doping [Fig. 3(e)]. This effect is more pronounced at high La substitution. Figure 3(f) shows the bond distance Ba–O(1) and the distance of Ba atom from the basal plane as a function of La doping x. The Ba–O(1) bond is increasing with x, in accordance with the modifications observed for the a, b axes [Fig. 2(b)]. The Ba atom is slightly shifted, with a jump at $x=0.8$, towards the basal plane with increasing La doping. The observed change at $x=0.8$ agrees with the corresponding modifications of the apical oxygen O(1) [Fig. 3(c)]. The overall shift of the Ba atom (0.02 Å) is much smaller compared to the corresponding one of the Cu(2) atom (0.07 Å). This indicates that the ionic size effect is more pronounced in the central Cu(2)–Cu(2) cube of the triple-perovskite unit cell while changes in the Ba cube could be induced by additional effects besides the size-effect.

Bond valence sum (BVS) at the Y/La and Ba site has been calculated according to Brown[17] (Fig. 4). The individual bond valences have been calculated using the relation $S_i = \exp[(R_0-R_i)/B]$, where R_0 has a characteristic value for a given cation–anion pair, R_i is the interionic distance, and B is a universal constant having the value 0.37 Å. The atomic bond valence V is obtained by summing up the bond valences associated with a particular ion, given by $V=\Sigma S_i$. The value of R_0 for Ba^{2+}–O^{2-} was chosen to be 2.297 (Ref. 18) and corresponding values for the R^{3+}–O^{2-} bonds were taken from Ref. 17. In the strained structure of the Y123 the BVS values at the rare earth and barium ions are indicative of internal strains. A bond valence sum for Y/La site greater than the nominal +3 is indicative for an ion that is too large for the central Cu(2)–O cage of the triple-perovskite structure. The stress in this case can be partially relieved by the modification of the Cu(2)–O–Cu(2) bond angles. Larger values for the strain and thus for BVS are expected when the larger La replaces the smaller Y. The observed increase in BVS is not linear with La doping x. For $x \geqslant 0.5$ BVS at the La/Y site increases considerably above +3 and saturates to a high value for $x \geqslant 0.8$ [Fig. 4(b)].

At small La substitution ($x \leqslant 0.2$) the BVS value of the Ba site is slightly increasing from the initial value of 2.17, indicating that the La substitution induces more compressive stress at the Ba site [Fig. 4(a)]. For intermediate values ($0.2<x \leqslant 0.7$) a systematic decrease is observed indicating the partial release of compressional stress. At higher La concentrations the BVS remains roughly equal to 2 and smaller than the corresponding in the Y123 cell in agreement with the results obtained for the R123 compounds by Ramesh *et al.*[6] In the case of Y123 Brown[18] has observed that the Ba atom is too large for the Cu–O framework at $y=7$ and too small at $y=6$, so that the valence sums at the Ba site are lower than the nominal +2 valency for lower oxygen contents while a linear increase occurs with increasing oxygen

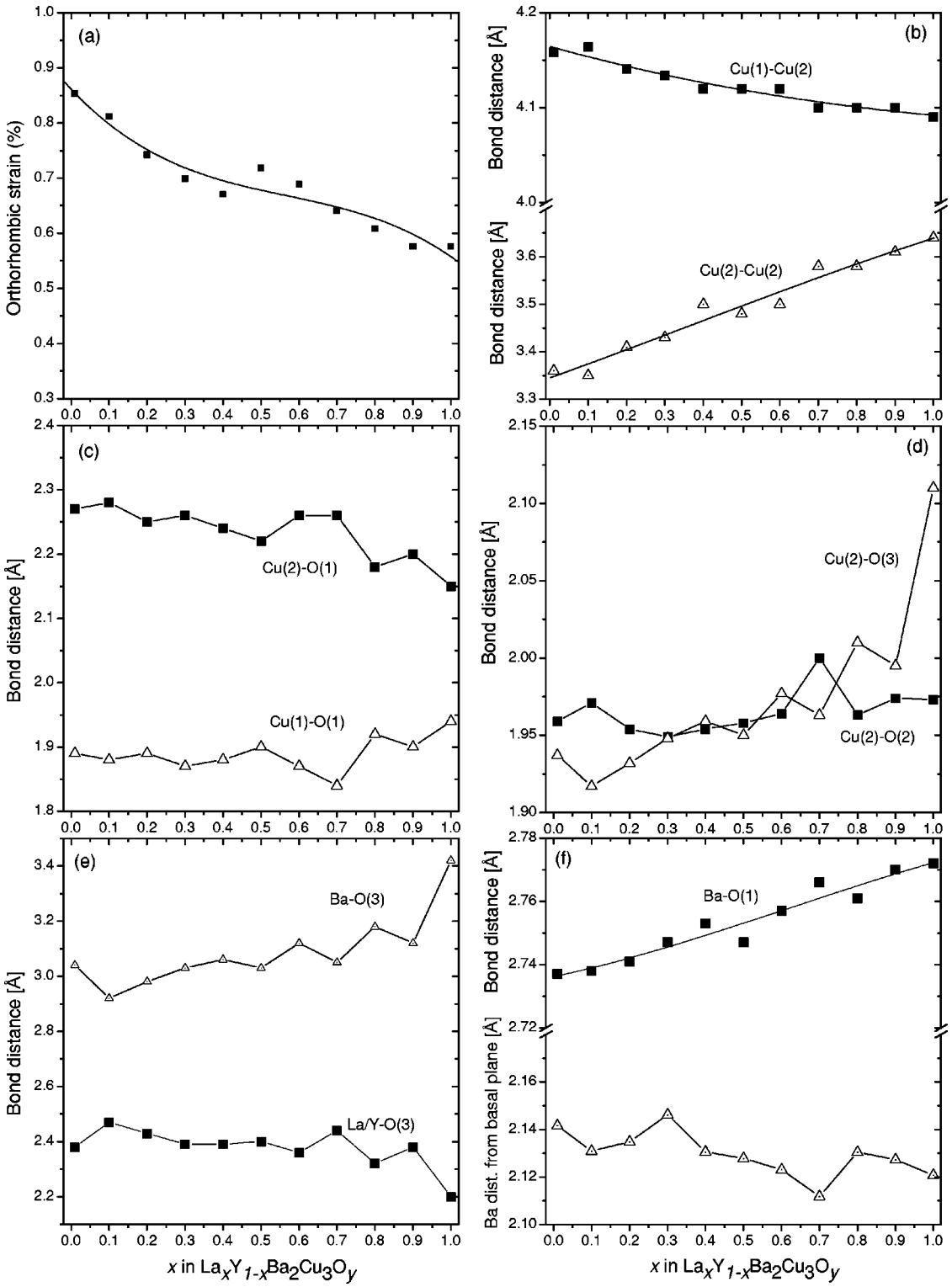

FIG. 3. Dependence of the orthorhombic strain (a), bond distances Cu(2)–Cu(2), Cu(1)–Cu(2) (b), bond distances Cu(2–O(1), Cu(1)–O(1) (c), bond distances Cu(2)–O(2), Cu(2)–O(3) (d), bond distances Ba–O(3), Y–O(3) (e), bond distance Ba–O(1) and Ba atom distance from the basal plane (f) of the (Y–La)123 compounds on the La content *x*.

content. The Ba atom in the optimally doped and overdoped Y123 structure is therefore in a state of compressional stress with a BVS value ≈ 2.2. Taking into account this linear dependence, the effect of oxygen content variation among our samples on the BVS values of Ba has been estimated. The results showed that the features observed at $x \approx 0.2$ and $x \approx 0.5$ in Fig. 4(a) become even more pronounced. This indicates that the observed changes in BVS at the Ba site can be attributed to the La doping. The partial release of stress at the Ba site, resulting in a BVS value $+2$ for the pure La123

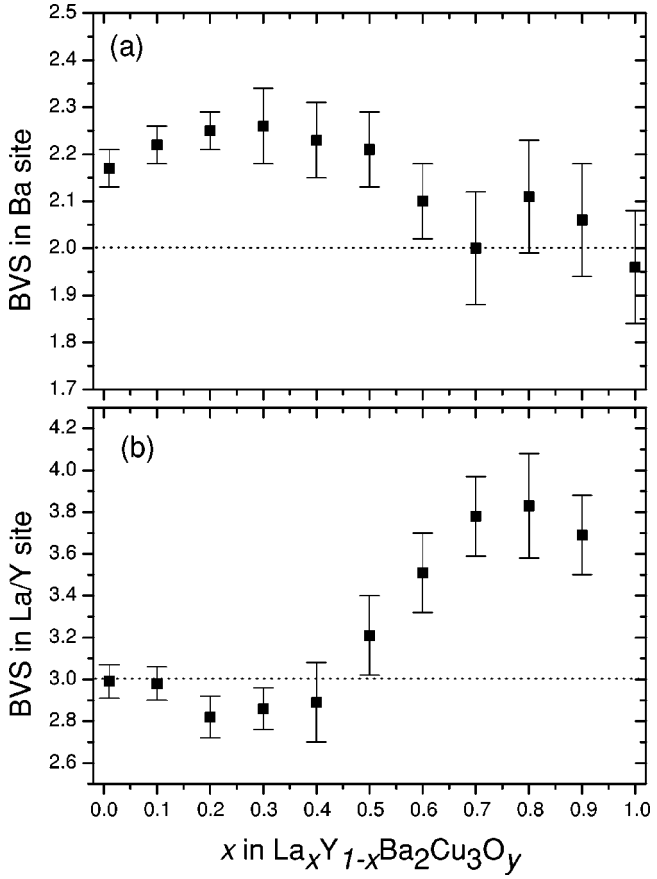

FIG. 4. Bond valence sum (BVS) values for the Ba (a) and the Y/La atoms (b) as a function of La content x for the (Y–La)123 compounds.

phase, could be understood as a partial replacement of the bigger Ba ($r=1.52$ Å for coordination 10) by the smaller La ($r=1.27$ Å for coordination 10). The observed modifications of Ba BVS value correlate with the formation of the La123 subphase as discussed below.

Typical Raman spectra for the two scattering polarizations are presented in Figs. 5(a) and 5(b) for selected La concentrations. In the low energy region of the zz polarization the phonon due to the Ba atoms appears as a double peak at high La concentrations ($>80\%$). The average peak position is located between the energy of the Ba mode in pure optimally doped Y123 and another mode energy at 126 cm^{-1} [Fig. 6(a)]. This additional peak was also detected in oxygen deficient $YBa_2Cu_3O_x$ samples[19] and corresponds to a disorder induced mode. In Y123 the disorder is induced from the loss of the chain oxygen, while in the present case of fully oxygenated samples it can be activated by the La substitution for Ba. From Fig. 6(a) we observe that the additional mode appears mainly at $x=0.2$, 0.6, 0.9, 1.0 and to a lesser degree for $x=0.7$. A similar behavior is observed in the dependence of the Ba phonon width on the La concentration [Fig. 6(b)].

Another weak mode appears at ≈ 160 cm^{-1} close to the phonon due to the Cu(2) atoms (at 150 cm^{-1}) of the CuO_2 planes. A similar peak has been observed in pure Y123 with decreasing amount of oxygen and it can be related with the disorder introduced with the oxygen deficiency. The peak

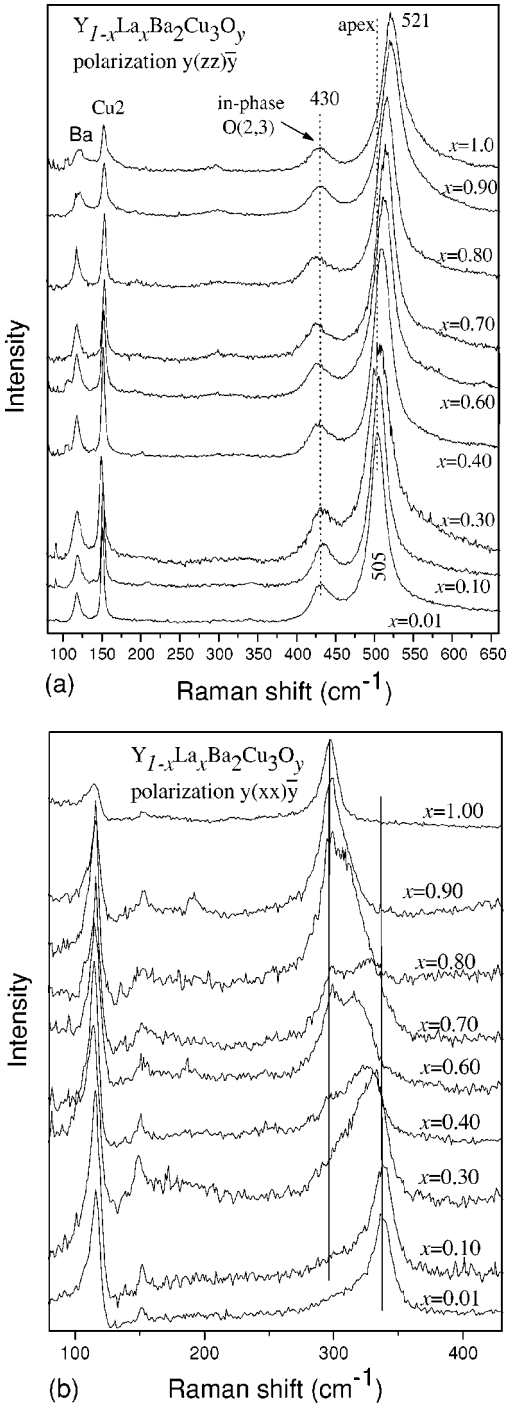

FIG. 5. Typical room-temperature micro-Raman spectra in the $y(zz)\bar{y}$ (a) and $y(xx)\bar{y}$ (b) scattering polarizations for selected (Y–La)123 concentrations.

position of phonon due to Cu(2) starts increasing with La for $x>0.2$ up to $x=0.8$, while its energy is reduced for pure La123 [Fig. 6(a)]. Its width shows the same behavior as the width of the Ba phonon [Fig. 6(b)].

In the high energy part of the same polarization spectra [Fig. 5(a)] the phonon due to the plane oxygen atoms O(2,3) remains almost constant in energy [Fig. 6(a)]. The energy of this phonon is very sensitive to the amount of oxygen[19] and corresponds to samples with optimum to overdopped oxygen

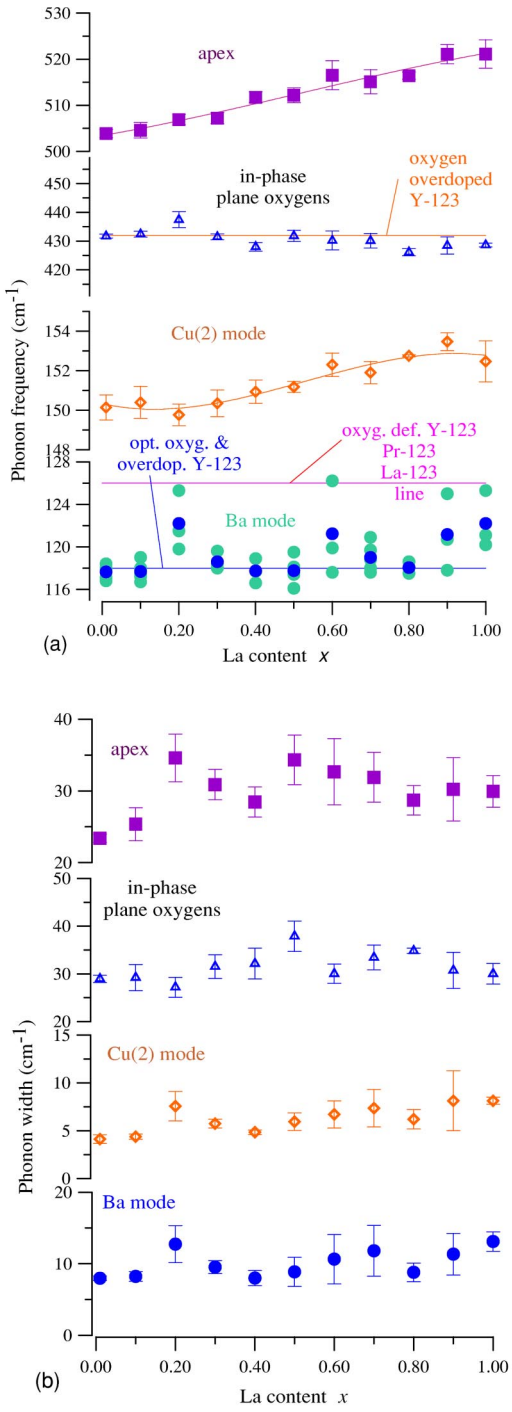

FIG. 6. "(Color online)" variation of the energy (a) and linewidth (b) of the A_g symmetry Raman active phonons with the La content x in the (Y–La)123 compounds.

concentration,[19] in complete agreement with the measurement of the oxygen content in the samples. Its width remains roughly contant except for $x=0.5$ [Fig. 6(b)]. The phonon at ≈ 503 cm^{-1} due to the apical oxygen gradually shifts to higher energies with increasing amount of La [Fig. 6(a)]. This must be due to the decreasing of the bond distance Cu(2)–O(1). A similar behavior has been observed in pure Y123 with increasing amount of oxygen doping.[19] The width of the apex mode shows a pronounced increase by 50% compared to the pure Y123 for $x=0.2$ and 0.5 [Fig. 6(b)].

In the other scattering polarization, the low energy modes due to the Ba and the Cu(2) atoms are reduced in intensity, but remain asymmetric (Fano shape) due to their coupling with the carriers. The out-of-phase vibrations of the O(2,3) of B_{1g} symmetry show the maximum modifications with the rare earth substitution. While at low La content this phonon has the normal asymmetric Fano shape, with increasing La concentration another peak at ≈ 297 cm^{-1} starts to develop around 30% La [Fig. 5(b)]. This second peak gains intensity with La and it becomes the dominant one around 60%–70% La. At the same time the B_{1g} mode shifts to lower energies and looses intensity with the La substitution, but it can be clearly discriminated even for $x=0.8$ [Fig. 5(b)]. At $x=0.9$ mainly the mode at 297 cm^{-1} appears with a very small contribution at higher energies from another mode. For 100% La substitution only the mode at ≈ 297 cm^{-1} remains, which apparently is the B_{1g} phonon of the La123 compound. This phonon is more symmetric than in the pure Y123 [Fig. 5(b)], which is an indication for the reduction of carriers in the CuO_2 planes. This could be the reason of the reduced transition temperature to 74 K.

B. Discussion

The b, $c/3$ and V_{cell} dependance on x indicates that there is a deviation from the linear Vegard's law expected when a solid solution is formed. The dependence of the Y123 lattice constants and volume on the oxygen nonstoichiometry varies in the optimum to overdoped region with the conditions of the synthesis.[20] The c lattice constant and V_{cell} decrease linearly with increasing oxygen content when Ba-carbonate is used as a precursor (Ref. 5 and CAR samples in Ref. 20), while a minimum is observed at the onset of overdoped region ($y \approx 6.93$) for samples prepared by the expelling carbonate method (BAO samples in Ref. 20). The c lattice constant of the $Y_{0.99}La_{0.01}Ba_2Cu_3O_{7.07}$ sample and our synthesis conditions suggest that our samples should be compared to those of Ref. 5 and the CAR samples of Ref. 20. Taking into account this linear dependence we can reduce the effect of oxygen content variation on the c lattice constant values according to the CAR samples data. In that case the features observed in Fig. 2 become even more pronounced. Corrections made even according to the BAO samples data, show that the deviation from nonlinearity, although smoother, persists as well. The dependence of the plane Cu(2)–O bond distances and BVS values, as discussed previously, upon La dopping x support this feature and indicate that the structural modifications observed at $x \approx 0.2$, $x \approx 0.5$, and $x \approx 0.8$ can be attributed to La doping. The evolution of the phonon shape [Fig. 5(b)] is quite convincing that at intermediate La concentrations ($0.2 < x < 0.8$) there is a coexistence of two peaks. One with lower energy clearly corresponds to the B_{1g} mode of pure La123, because it remains constant in energy as in the $x=1$ composition [Fig. 5(b)]. The other one for $x=0$ is the B_{1g} phonon of Y123, which with increasing amount of La is drifting to lower energies. It is reasonable to assume that it is a mode that originates from a mixed

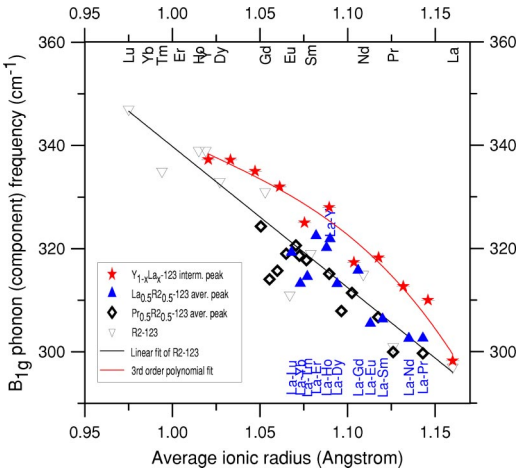

FIG. 7. "(Color online)" The dependence of the energy of the B_{1g} symmetry Raman active phonon on the ionic radius of (Y–La)123 and related compounds. The straight line is the best linear fit to the pure R123 compounds data (Ref. 21). The curve is a third order polynomial fit to the (Y–La)123 data.

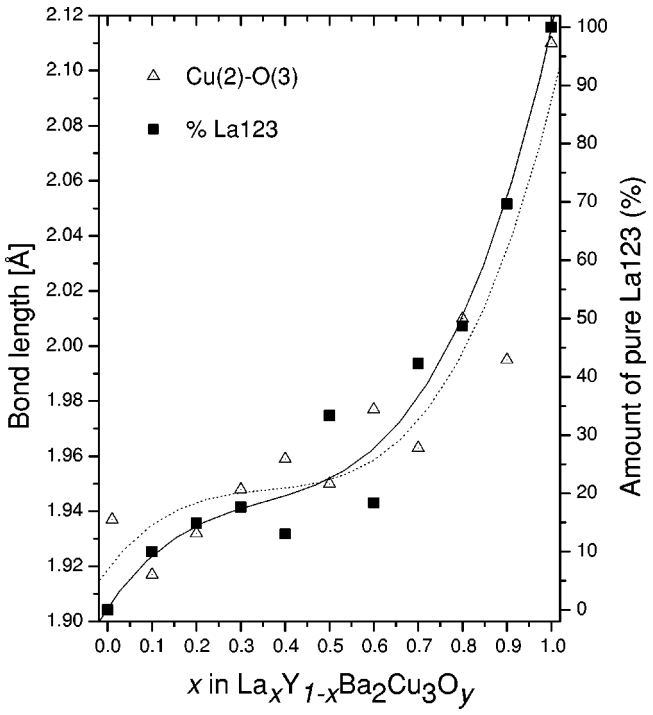

FIG. 8. The amount of pure La123 subphase in the sample, as estimated from the peak position of the B_{1g} symmetry Raman active phonon for the intermediate phase in comparison with the dependence of the Cu(2)–O(3) bond distance on the La content x for the (Y–La)123 compounds. Solid (doted) line is a third order polynomial fit to the La123 [Cu(2)–O(3) distance] data.

Y–La123 ($Y_{1-x}La_xBa_2Cu_3O_y$) phase with varying amount of La. Therefore the data show a mixture of one- and two-mode behavior. Figure 7 shows the peak position of the B_{1g} mode of the intermediate phase plotted vs the average ionic radius together with the results of the pure R123 phases. The latter have been experimentally observed to follow a linear dependence on the R ionic radius.[21] The average B_{1g} mode of the $R1_{0.5}R2_{0.5}Ba_2Cu_3O_x$ phases show a similar behavior.[8,22] Our end point data Y–La123 coincide with the previous measurements, but the rest of the data have a tendency to lie at higher energies than the pure R123 or the mixed compounds $R1_{0.5}R2_{0.5}Ba_2Cu_3O_x$. This behavior cannot be due to a variation in oxygen concentration among the samples, since such a change in oxygen concentration would not modify the energy of the B_{1g} mode.[19] The presence of the lower energy mode, which corresponds to the La123 phase indicates that part of La is used in this pure phase and the mixed $Y_{1-x}La_xBa_2Cu_3O_y$ phase must have less than the nominal amount of La. This explains the deviation of the mixed phase phonon energy from the corresponding value of the pure R123 in Fig. 7. From the peak position of the intermediate phase, one can calculate the average ionic radius this value would correspond to if it followed the linear best fit to the R123 data. From these values one can then estimate the amount of pure La123 present in the samples (Fig. 8). It is clear that, under this assumption of linear dependence of the B_{1g} phonon energy with x, above roughly 20% nominal La concentration, the amount of this La123 phase saturates and increases again above 60%. In this figure we have also included the changes of the interatomic distance Cu(2)–O(3) [Fig. 3(d)] which correlate with the changes of the estimated amount of pure La123 phase.

One is therefore forced to assume a separation into two phases; one phase of pure La123 and the intermediate $Y_{1-x}La_xBa_2Cu_3O_y$. The variation of the transition temperature with La content agrees well with this separation into phases, since there are similar changes in T_c; at $x \approx 0.2$ there is a drop in T_c, then a saturation up to $x \approx 0.6$ and a drop again with the further increase of La substitution [Fig. 1(b)]. The variation of T_c looks like being an average between the lower transition temperature of pure La123 and a constant one of the intermediate phase, not being proportional to the amount of La. At $x \approx 0.2$ there is a stepwise increase of the ΔT_c as well [Fig. 1(b)], which apparently reflects the development of the second phase. The ΔT_c remains large even for the end element La123 [Fig. 1(b)], but this is expected from the reduced amount of the superconducting state in this compound (Table I).

From the concentration dependence of all phonons studied, characteristic modifications have been observed in the width and energy mainly at $x \approx 0.2$ and $x \approx 0.8$, which may reflect crystallographic changes [Figs. 2(b) and 3].

A phase separation such as observed by Raman spectroscopy, can be interpreted as compositional inhomogeneity at the La/Y site in the microcrystalls which manifests itself as microstrains in the crystallites. In order to study the microstrains of the crystallites, line broadening analysis of the XRD Bragg reflexions has been used. Due to the line overlapping and generally low broadening in the pattern of the Y123 structure it is very difficult to apply methods of line deconvolution. We have thus applied the more simple method of integral breadth to determine the upper limit of apparent strains.[23] A silicon standard has been used to determine the instrument profile characteristics U,V,W from Rietveld analysis and the FWHM(2Θ) of the instrumental profile us-

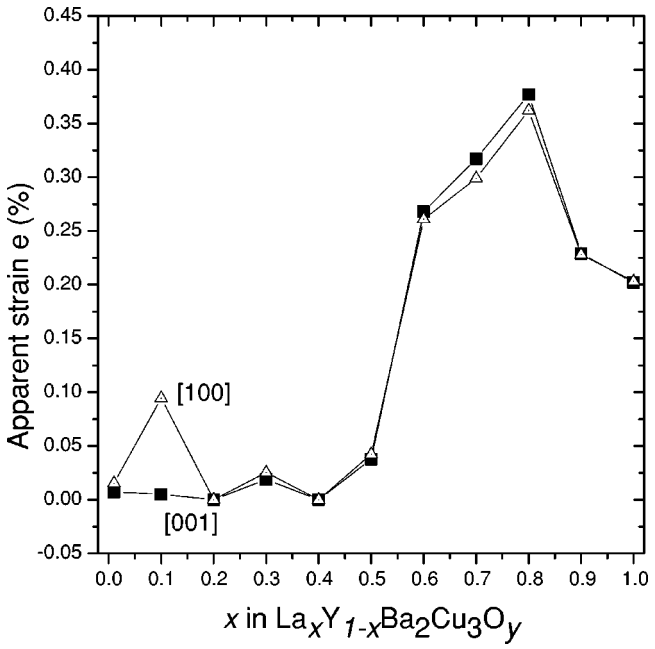

FIG. 9. The upper limit of apparent strain e (%) along the [001] and [100] directions as a function of the La content x in the (Y–La)123 compounds.

ing the Caglioti relation.[12] The sample broadening has been obtained from the experimental assuming a Gauss-type instrumental broadening,

$$(\mathrm{FWHM}_{\mathrm{samp}})^2=(\mathrm{FWHM}_{\mathrm{exp}})^2-(\mathrm{FWHM}_{\mathrm{ins}})^2.$$

The corresponding integral breadths β_{samp} have been calculated for the 00l and h00 reflections using the program BREADTH.[23] This program enables the calculation of the mean crystallite size (L) and the upper limit of strain (e), assuming a Gauss-Gauss, Cauchy-Gauss or Cauchy-Cauchy-type distributions for size and strain, respectively. Analysis of all samples showed that physically meaningfully results are obtained if one assumes Cauchy models for both size and strain, so that integral breadth $\beta_{\mathrm{samp}}(2\Theta)$ is given by the following expression:

$$\beta_{\mathrm{samp}}(2\Theta)=\beta_{\mathrm{size}}(2\Theta)+\beta_{\mathrm{str}}(2\Theta)=\frac{\lambda}{L\cdot\cos\Theta}+4e\cdot\tan\Theta,$$

where λ is the x-ray wavelength.

No significant contribution to the peak broadening has been obtained from crystallite size. The upper limit of strain along the [001] and [100] directions as a function of La doping is presented in Fig. 9. Microstrains are very low for the small substitution limit and are increasing for $0.2<x<0.8$. For the latter values of x, compositional inhomogeneity of samples is high due to phase separation observed from the Raman spectra and microstrains are expected to be more pronounced. Thus the large microstrain for $0.2<x<0.8$ is an indication of the coexistence of two phases, i.e., the inhomogeneous distribution of La at the Y site (phase separation). A decrease of microstrains is observed for the high substitution limit ($x=0.9,1.0$). For those samples more homogeneous La123 crystallites are expected to be formed according to the Raman data. Microstrains can probe the presence of phase-separated regions and/or crystal defects. In the La123 sample, microstrains are higher compared with those of the Y123 crystals. This can be interpreted either by a higher density of extended crystal defects or as a coexistence of orthorhombic Ba-rich and tetragonal La-rich phases, i.e., the inhomogeneous distribution of La at the Ba site. The values of microstrains obtained from our analysis are in general comparable with values (0.05%–0.3%) reported in literature for the Y123 system.[24,25]

One question has to be answered: what are the critical concentrations for the formation of the subphases. The crystallographic and the Raman data show three characteristic La concentrations, where structural changes are observed. For $x\approx0.2$, $x\approx0.5$, and $x\approx0.8$. The first value is the concentration where there is an inflection of the c-axis dependence on x [Fig. 2(b)], the BVS of Ba and Y/La show a local extreme (Fig. 4), the transition temperature decreases [Fig. 1(b)], the dependence on x of the phonon energy due to the Cu(2) atom starts increasing [Fig. 6(a)], and the phonon widths show sudden increases [Fig. 6(b)]. Besides, it is the concentration where the two plane Cu(2)–O bonds tend to become equal, and there seems to start the separation into two phases as judged from the Raman data (Fig. 5). At $x\approx0.5$ the BVS of Y/La starts increasing considerably above the value $+3$ (Fig. 4), as the apparent strain does (Fig. 9). Taking into account the BVS dependance on ionic radius of the R123 compounds,[6,7] we can see that for $x\approx0.5$ the average ionic radius of Y–La123 corresponds to BVS $\approx+3$. At this concentration therefore the average ionic radius of Y–La is such that the central cage is critically unstrained supporting the formation of a mixed Y–La123 phase. At $x\approx0.5$ the splitting of the B_{1g} mode in two peaks is obvious (Fig. 5) and T_c begins to drop [Fig. 1(b)]. In the range $0.2<x<0.7$ the amount of La123 seems to remain constant (Fig. 8) and only the intermediate phase increases. At $x\approx0.8$ the apparent strain drops (Fig. 9), the BVS of Y/La saturates [Fig. 4(b)], the Cu(2)–O(3)bond distance increases abruptly [Fig. 3(d)] and the c-axis dependence on x saturates [Fig. 2(b)] as does the dependence of the Cu(2) phonon energy [Fig. 6(a)]. In the Raman spectra (Fig. 5) the double peak structure is replaced by the spectrum of pure La123, its amount increases abruptly (Fig. 8), and the dependence of Cu(2) phonon is modified.

Our results can be consistently understood if one assumes that the separation into phases is driven mainly by the strain due to the difference in the ion sizes and that La has replaced Ba in small amounts only in the pure La123 phase reducing its transition temperature. In the samples with small La concentrations, the carriers will be localized at random sites (of the pure La123 phase) due to this La for Ba substitution. With the addition of La, more pure La123 cells will be created and at some critical concentration these will be enough in number to arrange themselves and create a subphase with lower T_c. Apparently this happens around 20% concentration in La. This does not imply that all 20% of unit cells with La at the site of Y have localized carriers, since only in a portion of them this happens. Until this concentration the

transition temperature is not modified, but for $x \geqslant 0.2$ the T_c will be an average between the T_c of the constant amount of the pure La123 phase and the rest of the compound with the high T_c. With the further increase of La the existence of two phases is more apparent as the Raman data show (Fig. 5). Above this concentration, probably the localized carriers of the pure La123 phase are enough in number to play some role in the phase separation mechanism by creating clusters similar to those observed in $Pr_{1+x}Ba_{2-x}Cu_3O_{7+\delta}$ by Grevin *et al.*[26] Until $x \approx 0.5$–0.6 the strain is minimized by the phase separation mechanism, but at higher concentrations even the intermediate phase is strained and the system prefers to create mainly the pure La123 phase. At $x \approx 0.8$the unit cells with mixed Y/La structure are few enough to stop producing clusters (as the La123 clusters that occurs at $x \approx 0.2$) and the system behaves mostly as pure La123, with decreased T_c because of the La replacement of selected Ba sites. Therefore there is a further decrease of the transition temperature and the other effects described above.

The variation of the amount of pure La123 with the nominal amount of La implies that the reduction in the T_c is associated with the development of the pure La123 phase and not with the total amount of La. Furthermore, the increase of La123 phase above $x \approx 0.8$ (Fig. 8) correlates with the considerable increase of the satellite peak at 126 cm^{-1} [Fig. 6(a)], which we believe it is due to a disorder at the Ba site. This justifies our assumption that La substitutes for Ba in the pure La123 phase only and this substitution is related with the reduction in T_c. Our results would very well explain the earlier observations of Ganapathi *et al.*[9] on the superconductive properties of $La_xY_{1-x}Ba_2Cu_3O_{7-\delta}$.

If the above assumptions turn out to be correct, they would imply that the phase separation is induced by the strains developed by the different size of the Y and La atoms but also affected by the internal strains due charge redistribution. Therefore, the mechanism could be different in the Pr substitution for Y, though the ion size of Pr is only slightly smaller than La. As observed,[8] $Pr_{0.5}R_{0.5}Ba_2Cu_3O_{7-\delta}$ compounds have different behavior of the interatomic distances compared to the $La_{0.5}R_{0.5}Ba_2Cu_3O_{7-\delta}$, indicating that the internal strains are due to different mechanisms in the two systems.

C. Conclusions

We have studied the effect of La substitution for Y in the $YBa_2Cu_3O_{7-\delta}$ superconductors. Based on the XRD measurements we find characteristic changes at nominal La substitutions 20%, 50%, and 80%, which correlate with modifications in the Raman spectra and the transition temperature. From the behavior of the B_{1g} mode and the XRD measurements we conclude that two phases are created with the La substitution, an intermediate one $Y_{1-x}La_xBa_2\,Cu_3O_y$ with less than the nominal La concentration and another, which seems to correspond to a pure $LaBa_2Cu_3O_y$ phase. The amount of this pure phase correlates very well with structural modifications and those observed in the transition temperature. Based on the Raman spectra and the XRD data, we propose that the reduction in T_c is driven by the La substitution for Ba that occurs in the pure La123 phase. This amount of substitution for Ba seems to be the same in all La concentrations and only the relative percentage of the pure La123 is changing among the different compounds. Therefore, phase separation effects should be taken into account when interpreting superconductive properties in the solid solution $R_{1-x}R'_xBa_2Cu_3O_y$ systems.

ACKNOWLEDGMENTS

Work was partially supported by the Special Research Account of University of Athens. Thanks are due to Dr. D. Niarchos (NCSR ''Demokritos'') for the SQUID measurements.

[1] G.D. Chryssikos, E.I. Kamitsos, J.A. Kapoutsis, A.P. Patsis, V. Psycharis, A. Koufoudakis, Ch. Mitros, G. Kallias, H. Gamari-Seale, and D. Niarchos, Physica C **254**, 44 (1995).

[2] M. Guillaume, P. Allenspach, J. Mesot, B. Roessli, U. Staub, P. Fischer, and A. Furrer, Z. Phys. B: Condens. Matter **90**, 13 (1993).

[3] T. Wada, N. Suzuki, A. Maeda, T. Yabe, K. Uchinokura, S. Uchida, and S. Tanaka, Phys. Rev. B **39**, 9126 (1989).

[4] M. Izumi, T. Yabe, T. Wada, A. Maeda, K. Uchinokura, S. Tanaka, and H. Asano, Phys. Rev. B **40**, 6771 (1989).

[5] J.D. Jorgensen, B.W. Veal, A.P. Paulikas, L.J. Nowicki, G.W. Crabtree, H. Claus, and W.K. Kwok, Phys. Rev. B **41**, 1863 (1990).

[6] S. Ramesh and M.S. Hegde, Physica C **230**, 135 (1994).

[7] S.V. Samoylenkov, O.Yu. Gorbenko, and A.R. Kaul, Physica C **278**, 49 (1997).

[8] M. Calamiotou, A. Gantis, D. Palles, D. Lampakis, E. Liarokapis, and A. Koufoudakis, Phys. Rev. B **58**, 15 238 (1998).

[9] L. Ganapathi, A. Kumar, and J. Narayan, Physica C **167**, 669 (1990).

[10] J. Karpinski, K. Conder, and E. Kaldis, Physica C **401**, 153 (1988).

[11] S. A. Howard, RIET, Department of Ceramic Engineering, University of Missuri-Rolla, MO 65401.

[12] R. A. Young, *The Rietveld Method* (International Union of Crystallography, Oxford University Press, Oxford, 1993).

[13] N. Guskos, V. Likodimos, C.A. Londos, V. Psyharis, C. Mitros, A. Koufoudakis, H. Gamari-Seale, W. Windsh, and H. Metz, J. Solid State Chem. **119**, 50 (1995).

[14] R.J. Hill and C.J. Howard, J. Appl. Crystallogr. **20**, 467 (1987).

[15] H.A. Blackstead, J.D. Dow, I. Felner, and W.B. Yelon, Phys. Rev. B **63**, 094517 (2001).

[16] W.E. Picket, Physica C **289**, 51 (1997).

[17] I.D. Brown and D. Altermatt, Acta Crystallogr., Sect. B: Struct. Sci. **41**, 244 (1985).
[18] I.D. Brown, J. Solid State Chem. **82**, 122 (1989).
[19] D. Palles, N. Poulakis, E. Liarokapis, K. Conder, E. Kaldis, and K.A. Muller, Phys. Rev. B **54**, 6721 (1996).
[20] E. Kaldis, in *Handbook of Physics and Chemistry of the Rare Earths*, edited by L. Eyring, K. A. Gschneidner, Jr., and B. Maple (North-Holland, Elsevier, Amsterdam, 2001), Vol. 31.
[21] H.J. Rosen, R.M. Macfarlane, E.M. Engler, V.Y. Lee, and R.D. Jacowitz, Phys. Rev. B **38**, 2460 (1988).
[22] G. Bogachev, M. Abrashev, M. Iliev, N. Poulakis, E. Liarokapis, C. Mitros, A. Koufoudakis, and V. Psyharis, Phys. Rev. B **49**, 12 151 (1994).
[23] D. Balzar, Program BREADTH, Journal of Research of the National Institute of Standards Technology.
[24] A. Williams, G.H. Kwei, R.B. Von Dreele, A.C. Larson, I.D. Raistrick, and D.L. Bish, Phys. Rev. B **37**, 7960 (1988).
[25] J. P. Singh, R. A. Guttschow, D. S. Kupperman, J. T. Dusek, and R. B. Poeppel, *High Temperature Superconducting Compounds III*, edited by S. Whang, A. Gupta, and E. Collings (TMS, AIME, Warrendale, 1991), p. 281.
[26] B. Grevin, Y. Berthier, P. Mendels, and G. Collin, Phys. Rev. B **61**, 4334 (2000).